Unravelling the nature, evolution and spatial gradients of active species and active sites in the catalyst bed of unpromoted and K/Ba-promoted Cu/Al_2O_3 during CO_2 capture-reduction

Tsuyoshi Hyakutake,[a,b] Wouter van Beek[c] and Atsushi Urakawa[a,*]

CO_2 capture-reduction (CCR) is a recently developed catalytic process that combines two critical functions of CO_2 utilization path in one process, namely CO_2 capture and subsequent transformation (e.g. reduction by H_2) into chemical fuels or intermediates such as CO. A bifunctional catalyst material is needed and the two functions are activated by means of an isothermal unsteady-state operation (i.e. gas switching). This work employs *operando* space- and time-resolved DRIFTS, XAFS, and XRD to elucidate the nature and functions of Cu and the promoters. Both unpromoted and K/Ba-promoted Cu/Al_2O_3 catalysts were studied to illuminate the active surface species varying along the catalyst bed. The K promotor was found to uniquely facilitate efficient CO_2 capture in the form of surface formates, dispersion of active metallic Cu and suppression of surface Cu oxidation. The CO_2-trapping efficiency of the K-promoted catalyst is so high that CO_2 capture takes place gradually along the catalyst bed towards the reactor outlet, hence creating large spatial and temporal gradients of surface chemical species. Understanding these features is of central importance to design efficient CCR catalysts. Furthermore, a completely different path for CO_2 reduction was evidenced for the unpromoted and Ba-promoted Cu catalysts where CO_2 can directly react with metallic Cu and oxidize its outer surface and thus releasing CO. These results also provide important new mechanistic insights into the widely investigated reverse water-gas shift reaction and the role that K and Ba promoters play.

Introduction

Convincing evidences show that carbon dioxide (CO_2) emission into the atmosphere, mainly by burning fossil fuels, induces global warming and climate changes.[1] At the same time, the irreversible consumption of fossil fuels also causes depletion of natural resources. One promising path to mitigate these problems is to close the carbon cycle by converting CO_2 into useful chemicals. Catalysis offers numerous possibilities and plays pivotal roles in converting CO_2 to a variety of products such as chemical fuels (e.g. methanol and methane), commodity chemicals (e.g. carbonates and polymers), and added-value chemicals (e.g. pharmaceutical chemicals).[2-7]

Although numerous paths to efficiently convert CO_2 have been demonstrated, most catalytic conversion technologies assume use of highly or relatively pure CO_2. CO_2 emitted from various industrial sources is generally found in the range of 3-13 vol% diluted in other gases such as N_2, O_2, water (vapour), NO_x and SO_x. It is very important to highlight that CO_2 capture and purification, needed for such processes, are energetically and economically demanding; it is expected that full CO_2 capture from power plants would increase the levelised cost of energy (LCOE) by 33-64%.[8] Therefore, it is of prime importance to develop technologies that are able to transform directly the diluted CO_2 available in industrial flue gas.
Chemical looping is a process concept which possibly allows efficient conversion of CO_2 in flue gas,[9, 10] although the process is relatively complex and high conversion efficiencies have not yet reached. Recently we have demonstrated that CO_2 capture and efficient conversion to syngas (a mixture of carbon oxides and hydrogen) can be achieved in one process using isothermal unsteady-state operation in the presence of a bi-functional catalyst.[11] In this process, a catalyst (e.g. Fe, Cr, Cu and K supported on $MgO\text{-}Al_2O_3$ mixed oxide) packed in a reactor first chemically captures CO_2. Subsequently, the stored CO_2 is reduced by switching to a hydrogen atmosphere into CO. Thus, the process was named CO_2 capture-reduction (CCR). The product gas contains CO and unreacted CO_2 and H_2, resulting in syngas of carbon oxides with hydrogen suited for e.g. methanol synthesis. Notably, high CO_2 capture efficiency above 99% was achieved. In an optimized system, the CO_2 capture and reduction period was about 100 s using 5.8% CO_2 in the capture phase at space velocity of 1620 mL g_{cat}^{-1} h^{-1} and pure H_2 at 3900 mL g_{cat}^{-1} h^{-1} in the reduction phase.[11]

Despite the excellent CO_2 capture and reduction efficiencies of the CCR process, there is no knowledge available about the underlying chemical processes and catalytically active sites and species. The investigation of these aspects is technically highly challenging because the active species and sites dynamically evolve upon CO_2 capture and reduction phases, thus requiring time resolution. Even great

spatial gradients of surface chemical species and also electronic states of active metal are expected to exist, because of the extremely high CO_2-trapping efficiency. It is therefore expected that the CO_2-capture front moves from the front position towards the end of the catalyst bed along the axial direction of the reactor. In the same manner, the reduction of captured CO_2 is expected to take place with a strong spatial gradient of dynamically varying surface species.

In this work we aim at elucidating the roles of active chemical elements using three model CCR catalysts, Cu/Al_2O_3 with and without K or Ba promotion, by three complementary space- and time-resolved techniques. The three techniques are diffuse reflectance infrared Fourier transform spectroscopy (DRIFTS) to shed light on surface chemical species, X-ray absorption fine structure (XAFS) to gain insights into the electronic structure of Cu, and X-ray diffraction (XRD) to understand the catalyst structures during CCR. The combination of these techniques is powerful in gaining chemical, structural, and electronic insights into the catalysts and involved species, thus facilitating to holistically understand the catalytic process. Such understanding drives rational catalyst and even process design when space-resolution on a reactor scale is added.[12, 13] Furthermore, multivariate analysis on massive and complex XAFS and XRD data was performed using multivariate curve resolution (MCR) to enhance the signal-to-noise, detect subtle spectral changes during CCR process and simplify the spectroscopic analysis of large data.[14-16] We found, during our extensive study to identify an effective CCR catalyst ($FeCrCu-K/MgO-Al_2O_3$), that Cu and K play a crucial role in CO_2 reduction and capture respectively. These catalysts were hence selected for this follow-up mechanistic study. Another less effective promoter for CO_2 capture, Ba, was also investigated to highlight the difference from the more effective potassium one. The function and exact roles of active sites and species at different axial positions of the catalyst bed at different time point in CCR cycle will be presented and discussed.

Results and discussion

CO_2 capture-reduction behaviour of unpromoted and K/Ba-promoted Cu/Al_2O_3

Figure 1 shows the CO_2, CO, and CH_4 concentration profiles obtained for unpromoted and K/Ba-promoted Cu/Al_2O_3 catalysts under CCR conditions, namely switching repeatedly between a gas flow of 4.4% CO_2 in He and that of pure H_2 at 350 °C. As a reference, a concentration profile measured at room temperature using a reactor filled with SiC ("blank") is also shown. The three catalysts could convert CO_2 to mainly CO and a minor amount of CH_4, obviously with very different product concentration profiles and also different levels of CO_2 capture capability.

The $Cu-K/Al_2O_3$ catalyst showed the desired behavior of a CCR catalyst; capturing CO_2 as a surface chemical species and upon switching to H_2 atmosphere reducing the surface species to produce CO. Especially during the first 60 s, CO_2 is almost fully captured (Figure 1, $Cu-K/Al_2O_3$). When the capture phase duration is reduced to 60 s the CCR process becomes efficient as almost all of CO_2 entering the reactor is captured during this period and reduced upon switching to H_2 atmosphere. We have chosen however a longer period of 310 s to understand the underlying chemical processes and highlight the differences among the three catalysts. The CO_2 capture efficiency during the CO_2 capture phase (the first 310 s) of the presented data is 48.4%, showing relatively high value under this non-optimized CCR condition. High selectivity to CO (93.4%) during the reduction phase was observed.

Cu/Al_2O_3 showed a markedly contrasting concentration profile compared to $Cu-K/Al_2O_3$ with a dominant formation of CO during the capture phase where only CO_2 (diluted in He) passed over the catalyst. According to the concentration profile and carbon balance, the CO_2 passing over the catalyst was spontaneously converted to CO. The conversion was higher during the initial period of the CO_2 capture phase. Upon switching to H_2, a small increase in CO concentration and a slight CH_4 formation were also observed, indicating that a small amount of CO_2 was captured over the unpromoted catalyst. A careful look into the CO profile of $Cu-K/Al_2O_3$ (Figure 1) also shows a small CO formation for the K-promoted catalyst during the capture phase after the CO_2 concentration in the stream started increasing (i.e. after 100 s).
On the other hand, the Ba-promoted catalyst ($Cu-Ba/Al_2O_3$) exhibited catalytic performance with mixed characteristics of Cu/Al_2O_3 and $Cu-K/Al_2O_3$, i.e. with notable formation of CO during the capture phase as well as upon switching to the reduction phase. The amount of CO_2 converted or chemically stored on $Cu-Ba/Al_2O_3$ during the capture phase was 11.4%. The value is higher than that observed for Cu/Al_2O_3 (7.4%) but remarkably smaller than that observed for $Cu-K/Al_2O_3$ (48.4%). The trapped CO_2 could be converted to CO in the reduction phase with lower selectivity (74%, calculated only from the produced CO and CH_4 in the

reduction phase) compared to Cu-K/Al_2O_3. These results above clearly show that Cu can effectively catalyse CO_2 reduction but in a very distinct manner under the unsteady-state condition in the absence or presence of the K or Ba promotors. The action of K promotion is unique and very effective in both CO_2 capture and its reduction upon switching to H_2. The function of K and the origin of CO_2 reduction activity of Cu were investigated in depth by space- and time-resolved spectroscopic techniques and discussed in the following sections.

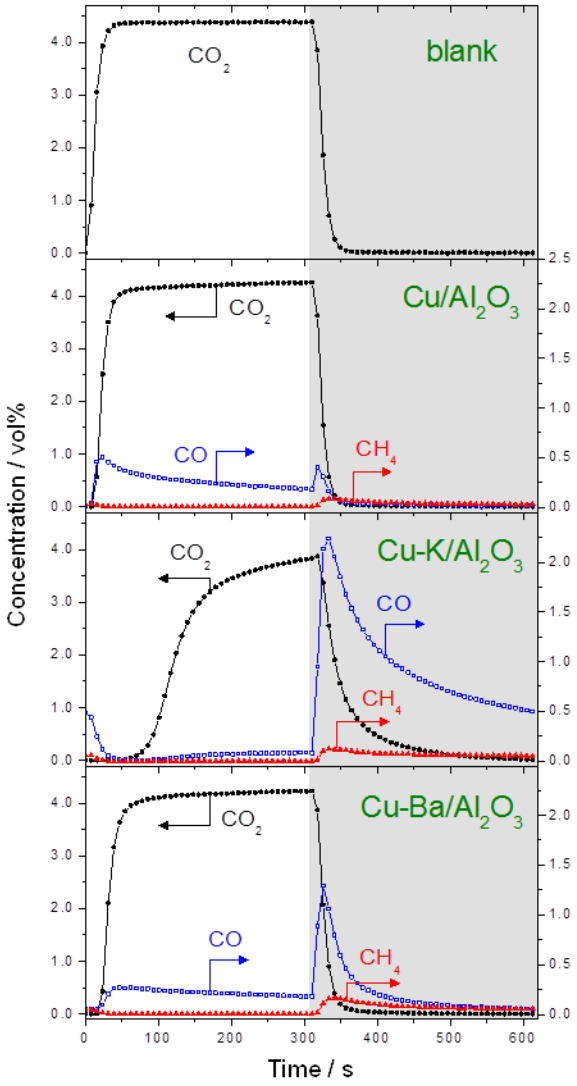

Figure 1. Concentration profiles of CO_2 and reduction products (CO and CH_4) during CCR operation at 350 °C with 4.4% CO_2 in He (in white) vs. 100% H_2 (in grey) at 50 mL/min at atmospheric pressure over inert SiC ("blank" performed at RT) and over unpromoted and K- and Ba- promoted Cu/Al_2O_3. The concentration profiles after stabilization (quasi-steady-state after a number of CCR cycles) are shown by averaging the concentration profiles of several CCR cycles.

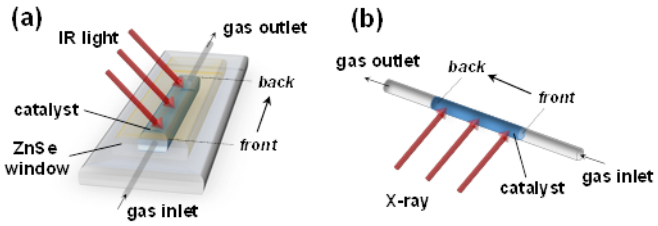

Figure 2. Schematic illustration of the (a) DRIFTS cell and (b) the XAFS/XRD capillary cell used for space- and time-resolved studies.

Space- and time-resolved spectroscopic study

In a CCR process, chemical processes taking place over a catalyst surface dynamically evolve due to the unsteady-state operation and periodic changes in the reactive atmosphere. To shed light on such processes, the use of time-resolved spectroscopy mimicking the nature of actions in the CCR reactor is of prime importance. Furthermore, large gradients in the concentration of surface chemical species and variations in the electronic structures of the active metal and promotors along the axial direction of the reactor may exist for good CCR catalysts. Therefore, we have employed three spectroscopic techniques, namely DRIFTS, XAFS and XRD, in a way that space- and time-resolution can be achieved using a specially designed DRIFTS cell and a capillary reactor for XAFS and XRD (Figure 2). Space-resolution was added by moving the whole cells while retaining the position of the optical components and the light path fixed.

DRIFTS

Figure 3 illustrates the four positions we have investigated along the catalyst bed and show time-resolved DRIFT spectra at the respective position for the three catalysts under CCR conditions. The catalyst amount and space velocity were adjusted (down-scaled compared to the catalytic tests) according to the size of the reactor channel and the catalyst bed.

The space- and time-resolved DRIFTS study clarifies a large spatial gradient of surface chemical species and their dynamic evolution for Cu-K/Al_2O_3. The surface species are assigned as a form of formates over K promoter as reported previously during CO_2 hydrogenation to CO and methanol using a similar catalyst.[17] It is important to highlight the movement of the CO_2 capture front; the formation of the surface formates starts early at the front position and is delayed towards the back position. At the back position, the formation of formates, thus CO_2 capture, was initiated at ca. 50 s. At the same time, the concentration of CO_2 in the effluent stream measured by MS increased. This clearly indicates a high efficiency of Cu-K/Al_2O_3 catalyst in chemically trapping CO_2 at the reaction temperature, thus resulting in the gradual movement of the CO_2 capture front along the flow direction. The reduction of the captured CO_2 to CO over Cu-K/Al_2O_3 proceeded slowly according to the MS profile. This is in accordance with the evolution of the surface formates for which slower reduction towards the back position could be recognized.

The DRIFT spectra of Cu-Ba/Al_2O_3 show also a clear formation of surface formates. The vibrational frequencies of the two major bands are red/blue shifted for the higher/lower frequency-bands, respectively, compared to those observed on Cu-K/Al_2O_3 (Figure 3). These differences are in accordance with the previous report and attributed to the observation of formates adsorbed on Al_2O_3 and Ba species in case of Ba-promotion, whereas formates on Al_2O_3 can be fully suppressed for Cu-K/Al_2O_3 likely due to high dispersion of K species over the Al_2O_3 surface.[17] The major difference observed between the DRIFTS spectra for K-and Ba-promoted catalysts is the spatial gradient. In case of Ba-promotion, no clear capture front was found and CO_2 capture at the back position was initiated almost at the same time as at the front position due to incomplete CO_2 capture by the catalyst. The reduction of surface formates was quickly completed for Cu-Ba/Al_2O_3 without notable spatial dependence.

In contrast, the DRIFT spectra of Cu/Al_2O_3 showed weaker IR absorption by the surface species. Some surface species were formed but they were less defined compared to the cases of the K/Ba-promoted catalysts. The surface species were also reduced very quickly, indicating the weak binding of the surface species and/or residing only at the outer surface layer leading to rapid reduction.

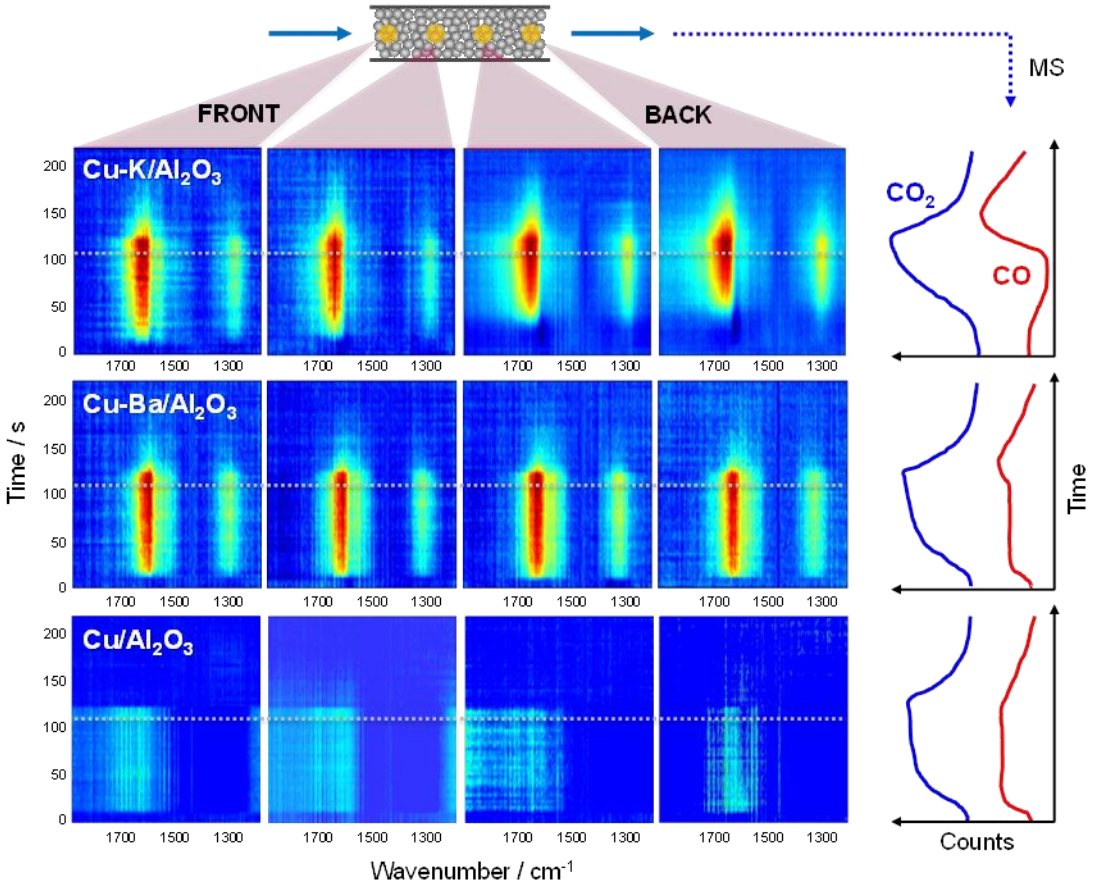

Figure 3. Evolution of surface chemical species clarified by space- and time-resolved DRIFT spectra under the CCR condition (1% CO_2 in He vs. 100% H_2, both at 10 mL/min for 110 s at 350 °C). CO_2 and CO concentrations (arbitrary unit) measured by MS are also presented. For CO (m/z=28) the contribution of CO_2 is subtracted. The scale of DRIFT spectra is in absorbance unit and colour code is normalized to the maximum value (dark red) of 0.010-0.015 for Cu-K/Al_2O_3, 0.008-0.010 for Cu-Ba/Al_2O_3 and 0.010 for Cu/Al_2O_3 for facile comparison.

XAFS

The electronic structure of Cu during CCR of the three catalysts and its possible temporal and spatial dependence were investigated by XAFS using the capillary reactor cell (Figure 2). The concentration profiles of CO_2, H_2 and CO in the effluent stream are presented in Supplementary Information (Figure S1). Figure 4 shows the XAFS spectra of the catalysts before the reaction (as-synthesized, fresh) and during CCR. Among the as-synthesized catalysts, some subtle differences in the edge peak features could be observed, but generally they remain in Cu(II) as expected from the XRD patterns shown later (Figure 6). Under the CCR condition after the reduction treatment, copper is reduced to Cu(0). The spectral difference among the three catalysts was again very small, although there were very slight differences in the near edge peaks when they were overlaid. These results indicate that during CCR, Cu species, at least the majority, remain Cu(0).

The changes in XAFS spectra were very small, virtually impossible to detect by eye the spectral changes or trends induced by the varying atmosphere of the CCR condition. In order to sense possible subtle spectral changes, we have employed multivariate spectral analysis, multivariate curve resolution (MCR), to extract pure component spectra from the kinetic resolution without reference.[14] The results of MCR analysis on the time-resolved XAFS spectra at the front position are presented in Figure 5. MCR successfully separated the original spectral data matrix into two temporally varying spectral components (Components 1 and 2). Although the differences between the two spectra are very small (Figure 5a), a clear periodic response to a specific type of gas atmosphere were confirmed (Figures 5b and 5c). The concentration of Component 1 increases in CO_2 atmosphere where CO is produced (Figure 1, Supplementary Information Figure S1), while the concentration of Component 2 increases in H_2 atmosphere. The characteristics of Component 1

spectrum in comparison to that of Component 2 are (i) less pronounced peak at the edge (ca. 8985 eV) and (ii) more enhanced absorption at the near-edge (ca. 8993-9004 eV). These spectral features are clear indications of a more oxidized Cu state of Component 1. Since both component spectra shows the strong character of metallic Cu (Cu(0)), the state of Component 1 is assigned to metallic Cu where only the outer surface is oxidized. Accordingly, Component 2 corresponds to fully reduced Cu. This explains well the observation under the CCR condition (Figure 1). Cu in Cu/Al_2O_3 is reduced under H_2 atmosphere and then surface is oxidized by CO_2, thus affording to produce CO in the absence of reducing gas like H_2.

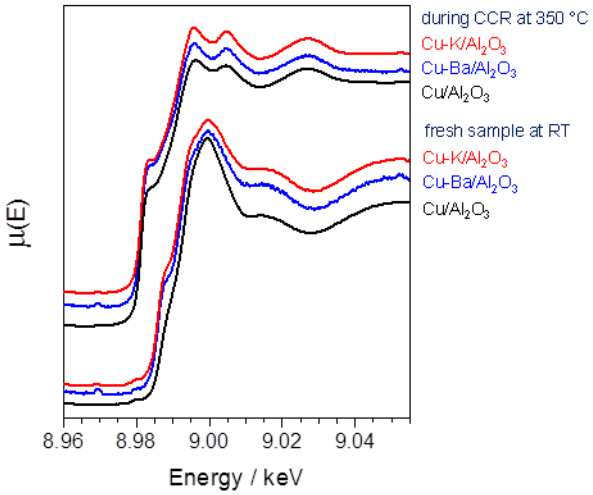

Figure 4. XAFS spectra of the unpromoted and K/Ba-promoted catalysts at Cu-K edge before the reaction (after synthesis) and during CCR at the front position (1% CO_2 in He vs. 100% H_2, both at 4.5 NmL/min and for 300 s thus 600 s of one CCR cycle at 350 °C). Representative spectra for the three catalysts under the CCR condition are shown by averaging the spectra over several CCR cycles.

Looking towards the back position of the catalyst bed, the same trends were confirmed with less pronounced changes in the spectral features and component concentration profile (Supplementary Information, Figure. S2). This is probably due to the fact that the concentration of reactive gases at the front position is the highest and their impacts on the oxidation state changes are larger, or the surface sites at more back positions are competitively covered (poisoned) by the produced CO at more front positions.

Cu XAFS spectra of $Cu\text{-}Ba/Al_2O_3$ are expected to show similar spectral changes to those of Cu/Al_2O_3 indicative of surface Cu oxidation according to the clear production of CO upon passing CO_2 (Figure 1). However, no clear changes could be detected, most likely due to higher X-ray absorption by Ba and consequent lower S/N when $Cu\text{-}Ba/Al_2O_3$ was studied under the same experimental condition. Under such circumstances, subtle changes and trends could not be firmly confirmed.

Furthermore, no changes in XAFS spectra were detected for $Cu\text{-}K/Al_2O_3$ at all positions of the catalyst bed despite the high S/N of the spectra. In this case, it is interpreted that the oxidation state of Cu is unchanged during CCR. Cu is present but it may be protected by K and its oxidation state is not influenced by the atmosphere change during CCR.

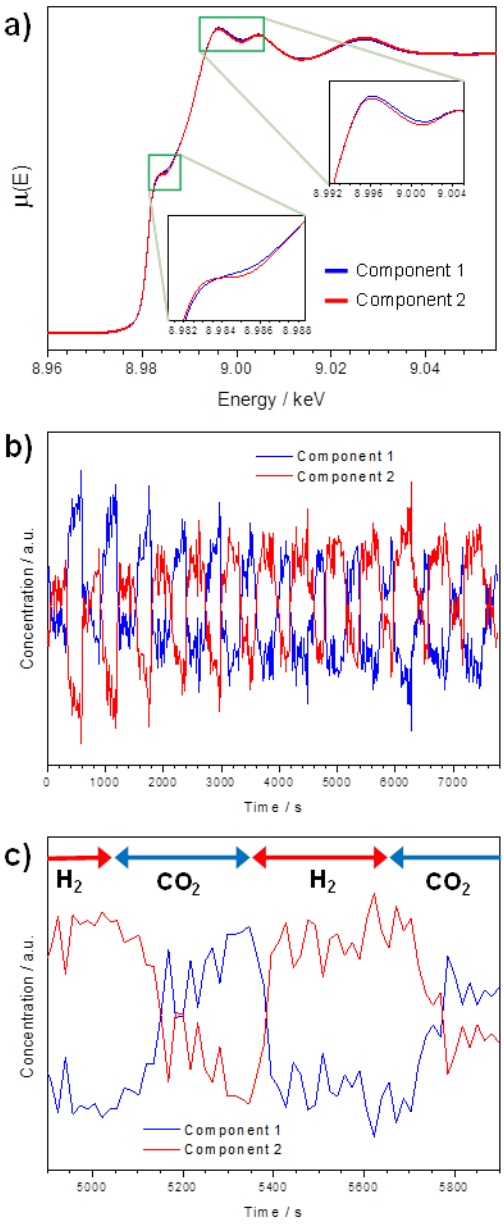

Figure 5. (a) Component XAFS spectra for Cu/Al_2O_3 at the front position during 13 CCR cycles extracted after MCR and (b) corresponding component concentration profiles. (c) Selected region of (b) to show the relation between the gas atmosphere in the capillary reactor and the concentration responses of the two spectral components. The experimental conditions are the same as described in the caption of Figure 4.

XRD

The structure of the three catalysts after the synthesis and under CCR condition was studied by space- and time-resolved XRD using the same capillary reactor system as in the XAFS study (Figure 2). Figure 6 shows the XRD patterns of the as-synthesized catalysts and also of the catalysts under the CCR condition (averaged patterns).

Identified crystalline phases of the fresh catalysts are mainly CuO and γ-Al_2O_3. For the K-promoted catalyst, there were additional small reflections observed, although the exact phase could not be identified. For the Ba-promoted catalyst, the phase of Ba species was identified to be $BaCO_3$. The Cu(II) state after the synthesis is in agreement with the XAFS study (Figure 4). After the reduction treatment and under CCR condition, the catalysts were reduced and Cu state became metallic. For Cu-Ba/Al_2O_3, the Ba species

remained $BaCO_3$ even under the reductive reaction condition. There were no other phases detected for Cu/Al_2O_3 and $Cu\text{-}Ba/Al_2O_3$ under the CCR conditions.

What is striking to observe is the feature of XRD pattern of $Cu\text{-}K/Al_2O_3$ under the CCR conditions (Figure 6), which exhibits completely different characteristics to those of Cu/Al_2O_3 and $Cu\text{-}Ba/Al_2O_3$. First, no reflections due to metallic Cu were observed, despite the fact that the oxidation state of Cu should be Cu(0) based on the XAFS study (Figure 4). Second, there was a strong increase in the baseline, indicating a formation of an amorphous and highly flexible structure. These two points indicate that K-promotion induces metallic Cu particles to be highly dispersed with the crystallite size too small to be detectable by XRD. The observation in DRIFTS suggested that the formates are in contact with K species rather than Cu or Al_2O_3 surface. Considering these observations and indications, K species may be melted or in a highly amorphous phase wherein metallic Cu (nano) particles are highly dispersed. In DRIFTS, the changes in the structure of chemical species on $Cu\text{-}K/Al_2O_3$ are evident, but in XRD and XAFS these changes are not detectable apparently. These results suggest that Cu particle size remains small and constant but the structure of K species dynamically changes by forming surface formates in an amorphous/ill-defined phase. Dynamic coverage of Cu particles by the K species may be crucial to block the Cu surface from oxidation which was observed for Cu/Al_2O_3 and $Cu\text{-}Ba/Al_2O_3$. The large crystallites of Cu and expected exposure of Cu surface are likely the favourable condition for surface oxidation by CO_2.

These dynamic contacts between K species and Cu may be the origin of the uniquely high CO_2 capture capacity by the K species and also of high reducibility of surface formates by the Cu species. In fact, oxidation of the Cu surface (i.e. surface oxidation by CO_2) for $Cu\text{-}K/Al_2O_3$ is minor but seems taking place once highly reactive surface sites are spent for CO_2 capture (e.g. after 60-100 s in Figure 1), coinciding with the moment when the CO_2 capture front reaches the end of the catalyst bed (e.g. after ca. 50 s in Figure 3). It is therefore very important to switch to the reduction phase once the capture front reaches the end of the catalyst bed not only to avoid CO_2 release but also to avoid CO formation during the capture phase.

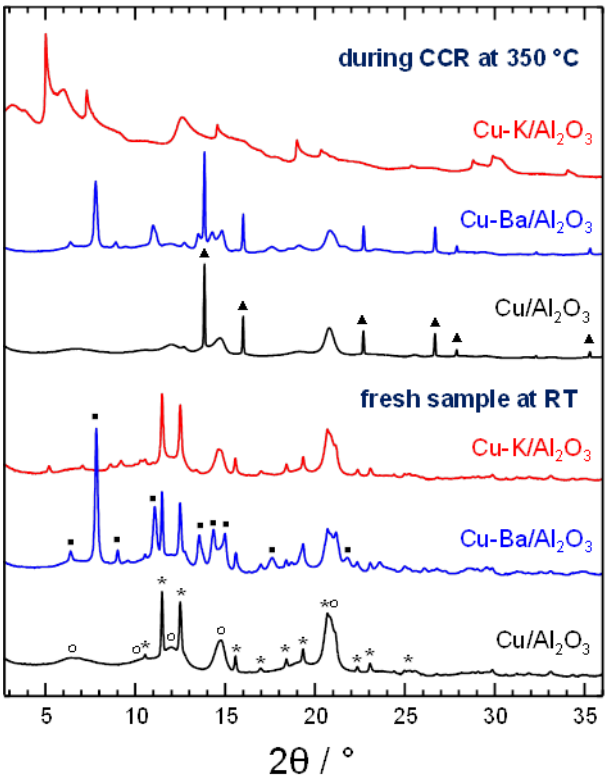

Figure 6. XRD patterns of the unpromoted and K/Ba-promoted catalysts before the reaction (materials as-synthesized) and during CCR at the front position (1% CO_2 in He vs. 100% H_2, both at 4.5 NmL/min and for 300 s thus 600 s of one CCR cycle at 350 °C). Representative patterns for the three catalysts under the CCR condition are shown by averaging the patterns over 2 CCR cycles. (*) CuO, (▲) Cu, (○) γ-Al_2O_3, (■) $BaCO_3$.

The search for the phases explaining the reflections observed for Cu-K/Al_2O_3 under the CCR condition was not successful, although a few peaks match with the structure of KOH·H_2O and the broad reflection angles are close to those of γ-Al_2O_3 with some shifts (Supplementary Information, Figure S3), suggesting possible structuring of K species and even possible changes in the Al_2O_3 structure. Moreover, for the three catalysts there were no obvious differences in the XRD patterns at the different locations of the catalyst bed during CCR cycle. After MCR analysis of the XRD data in a similar way as presented for the XAFS data (Figure. 5), 2-3 components could be identified with very similar patterns (not shown). When they are subtracted from each other after normalization, the difference pattern shows anomalous peak shapes, indicating that the peaks underwent some shifting. This may be caused by some structural changes but also temperature changes during CCR. Therefore, these data are not presented here and further studies for the structural identification is necessary, especially for Cu-K/Al_2O_3, for more unambiguous identification of the state of Cu, K and Al in the catalyst under CCR condition.

Conclusions

The first detailed mechanistic investigation on CO_2 capture-reduction (CCR) process was performed using three model catalysts, unpromoted and K/Ba-promoted Cu/Al_2O_3 catalysts, by means of catalytic tests and space- and time-resolved spectroscopy and diffraction, in some cases combined with multivariate spectral analysis. The desired CCR function and activity could be introduced upon K-promotion. The uniqueness of K-promotion was attributed to its amorphous nature under the reaction conditions which facilitated Cu to be very small and highly dispersed in a specific interaction with K species, preventing Cu from surface oxidation likely due to the coverage of K species over Cu surface. The unique state of K species allowed efficient CO_2 capture from a diluted CO_2 stream. The capture efficiency was so high that CO_2 capture front could be created and travelled from the front to the end of the catalyst bed as the catalyst became saturated with trapped CO_2. The captured CO_2 as formates was successfully reduced to CO by the function of the dispersed metallic Cu. In case of Cu/Al_2O_3 and Cu-Ba/Al_2O_3, the CO_2 capture efficiency was low. Rather, the Cu surface was oxidized and thus CO was produced during the CO_2 capture phase. The oxidized surface could be reduced in H_2 atmosphere. Although Cu-Ba/Al_2O_3 could capture some amount of CO_2, Ba-promotion was not efficient enough to fully trap CO_2 as confirmed by the formation of surface formates at the back position of the catalyst bed form the beginning of the capture phase, releasing significant amount of uncaptured CO_2 in the effluent stream. Hence, both Cu/Al_2O_3 and Cu-Ba/Al_2O_3 do not meet the requirements as CCR catalyst. At any rate, the surface oxidation and experimental evidence for the chemical process are important because of its high mechanistic relevance in reverse water-gas shift (RWGS) reaction.[18, 19] This study clearly shows the rich information gained by the unique combination of DRIFTS, XAFS, and XRD, with space- and time-resolution to understand materials and surface chemistry under working, *operando*, conditions towards rational catalyst design of chemical processes varying temporally and spatially in a reactor.

Experimental

Catalyst preparation

Cu/Al_2O_3 (10/90 wt%) was prepared by the incipient wetness impregnation method using copper(II) nitrate trihydrate (>98%, Alfa Aesar) and γ-Al_2O_3 (Alfa Aesar). It was then divided into three parts. The two parts were impregnated with potassium carbonate (>99%, Acros Organics) or barium acetate (>99%, Sigma-Aldrich) to obtain Cu-K/Al_2O_3 (11/10/79 wt%) or Cu-Ba/Al_2O_3 (15/10/75 wt%), respectively. The loading of K and Ba was balanced to have the same number of CO_2 capture sites assuming that CO_2 is captured in the form of K_2CO_3 and $BaCO_3$ with full utilization of surface and bulk K/Ba sites. The unpromoted and K- and Ba-promoted Cu/Al_2O_3 were dried overnight at 80 °C and calcined in air at 500 °C for 5 h.

Catalytic testing

The performance of the three catalysts was evaluated under CCR conditions in a fixed-bed reactor system. The set-up consists of four sections: (i) gas feed system, (ii) switching valve, (iii) reactor, and (iv) gas detection system. In (i), first CO_2 and He were premixed at a desired concentration regulating the flow rate entering to a dead volume at 3-5 bar pressure by means of mass flow controllers (MFCs, Bronkhorst). This method was used to have a flow with a stable CO_2 concentration. The flow of the gas mixture of CO_2 and He was then passed to the (ii) 4-way switching (selector) valve (Valco) at 50 mL/min by an MFC. Pure H_2 was also passed to the selector valve at 50 mL/min by means of an MFC and one of the two gases (CO_2+He

or H_2) was alternatingly passed to the (iii) reactor and the other gas was sent to exhaust. A catalyst was packed in a tubular fixed-bed reactor (I.D. 6.35 mm, O.D. 9.52 mm, length 15 cm) with ca. 10 cm in length. The effluent gas stream from the reactor goes into the (iv) gas detection system where transmission IR spectroscopy (ALPHA, Bruker) was used for fast detection and quantification of CO_2, CO, and CH_4 after confirming no other products were detected by gas chromatography. The selector valve switching and spectral acquisition for gas-phase detection were synchronized with LabVIEW software in order to facilitate the data analysis and also to precisely average over a number of capture and reduction cycles to increase the S/N of the data.
Before charging a catalyst to the reactor, it was pelletized, crashed and sieved to the size of 200-300 µm. 1.0 g of fresh catalyst was loaded in the reactor and reduced in the stream of pure H_2 at 450 °C for 1 h. After the prereduction, temperature of the reactor was set to 350 °C. The catalyst was then exposed to a number of CCR cycles (4.4 vol% CO_2 in He vs. 100 vol% H_2, 310 s each and in total 620 s per CCR cycle) at 350 °C until a reproducible concentration response of effluent gas components was attained. The presented catalytic performance was obtained by averaging 6 CCR cycles.

Space- and time-resolved DRIFTS

DRIFTS measurements were performed using a reaction cell, with a similar design to that reported previously,[20] mounted in a Praying Mantis (Harrick) optical accessory. In short, the catalyst-bed made of ca. 40 mg of catalyst material was placed as powder in a channel with the cross sectional area of 2x2 mm^2, resulting the bed length of ca. 20 mm. DRIFT spectra are recorded by detecting IR absorbance at the side of the catalyst-bed (Figure 2). By moving the whole cell, space-resolved study were made.[13] The spectra were collected with 4 cm^{-1} resolution on an FT-IR spectrometer (TENSOR 27, Bruker) equipped with a liquid-nitrogen-cooled MCT detector. The concentration profile of the effluent gas stream was monitored by mass spectrometry (OmniStar, Pfeiffer Vacuum). Prior to the DRIFTS measurements, a catalyst was reduced *in situ* at 350 °C in H_2 stream at 10 mL/min for 2 h. Subsequently, the catalyst was exposed to a number of CCR cycles (1 vol% CO_2 in He vs. 100 vol% H_2, both at 10 mL/min and 110 s) at 350 °C using the gas feed system and the selector valve of the catalytic tests. After attaining reproducible concentration response of effluent gas component, the DRIFT spectra were recorded every 3 s to follow the evolution of surface species. The spectral acquisition and gas switching were synchronized to facilitate averaging spectra of several CCR cycles into one cycle to improve the S/N.

Space- and time-resolved XAFS/XRD

XAFS and XRD experiments were performed at the Swiss- Norwegian Beamlines (SNBL, BM01B) of the European Synchrotron Radiation Facility (ESRF), France. The catalysts were pelletized, crashed and sieved to the size of 100-200 µm, and 8 mg of a fresh catalyst was loaded inside a quartz capillary (ID: 1.5 mm, thickness: 0.01 mm) with ca. 2 cm in length (Figure 2). A hot gas blower, covering the whole region where the catalyst is packed, was used to maintain the catalyst at the reaction temperature. Three locations at 1, 7.5, 14 mm from the beginning of the catalyst bed were examined by XAFS and XRD. Prior to the measurements, the catalyst was reduced *in situ* at 350 °C in 4.5 NmL/min of H_2 stream for 2 h. Subsequently, the catalyst was exposed to a number of CCR cycles (1 vol% CO_2 in He vs. 100 vol% H_2, both at 4.5 NmL/min and 300 s) at 350 °C. Switching between the two gas flows was performed with the 4-way selector valve. Both gas lines (CO_2 in He and H_2) were continuously flowing but alternatingly trough the sample. The pressure in both lines was kept constant at 1.0 bar by back-pressure regulators (Bronkhorst). After attaining a reproducible concentration response of the effluent gas species, XAFS spectra and XRD patterns were recorded and the effluent gas concentrations were recorded by mass spectrometer (OmniStar, Pfeiffer Vacuum).

XAFS spectra were recorded in transmission mode at the Cu K-edge using a double crystal Si (111) monochromator. A copper foil was used for energy calibration. One XAFS spectrum was acquired in ca. 15 s (ca. 20 spectra for the capture/reduction phase) and repeated for 10-15 CCR cycles.
XRD patterns were recorded on a large area 2D CMOS detector[21] with the incident X-ray at the wavelength of 0.50539 Å. The detector calibration was performed with the LaB_6 standard. One XRD pattern was acquired in 5 s (30 spectra for the capture/reduction phase) and repeated for 2 CCR cycles per catalyst-bed position per sample.

MCR

Multivariate curve resolution (MCR) analysis of the spectral data for the aim to separate spectral components in a blind manner (i.e. without reference spectra) by kinetic resolution were performed by the

algorithm implemented in MCR-ALS GUI 2.0[22] for MATLAB with a constraints of positive component spectra.

Acknowledgements

TH and AU acknowledge MINECO for financial support (CTQ2012-34153) and for support through Severo Ochoa Excellence Accreditation 2014-2018 (SEV-2013-0319). Recognition from the Catalan government (grant 2014 SGR 893) is acknowledged. We thank Research Council of Norway for funding of the 2D XRD detector through Synknøyt project (21840) and Repsol for kindly lending us the CCR reaction system to evaluate the catalysts.

References

1. IPCC, *Climate Change 2014: Synthesis Report. Contribution of Working Groups I, II and III to the Fifth Assessment Report of the Intergovernmental Panel on Climate Change*, Geneva, Switzerland, 2014.
2. H. Arakawa, M. Aresta, J. N. Armor, M. A. Barteau, E. J. Beckman, A. T. Bell, J. E. Bercaw, C. Creutz, E. Dinjus, D. A. Dixon, K. Domen, D. L. DuBois, J. Eckert, E. Fujita, D. H. Gibson, W. A. Goddard, D. W. Goodman, J. Keller, G. J. Kubas, H. H. Kung, J. E. Lyons, L. E. Manzer, T. J. Marks, K. Morokuma, K. M. Nicholas, R. Periana, L. Que, J. Rostrup-Nielson, W. M. H. Sachtler, L. D. Schmidt, A. Sen, G. A. Somorjai, P. C. Stair, B. R. Stults and W. Tumas, *Chem. Rev.*, 2001, **101**, 953-996.
3. D. J. Darensbourg, *Chem. Rev.*, 2007, **107**, 2388-2410.
4. M. R. Kember, A. Buchard and C. K. Williams, *Chem. Commun.*, 2011, **47**, 141-163.
5. X.-B. Lu, W.-M. Ren and G.-P. Wu, *Acc. Chem. Res.*, 2012, **45**, 1721-1735.
6. R. Martin and A. W. Kleij, *ChemSusChem*, 2011, **4**, 1259-1263.
7. A. Bansode and A. Urakawa, *J. Catal.*, 2014, **309**, 66-70.
8. IEA, 2013.
9. L.-S. Fan, L. Zeng, W. Wang and S. Luo, *Energy Environ. Sci.*, 2012, **5**, 7254-7280.
10. Y. A. Daza, R. A. Kent, M. M. Yung and J. N. Kuhn, *Ind. Eng. Chem. Res.*, 2014, **53**, 5828-5837.
11. L. F. Bobadilla, J. M. Riesco García, G. Penelás Pérez and A. Urakawa, *submitted*
12. M. A. Newton and W. van Beek, *Chem. Soc. Rev.*, 2010, **39**, 4845-4863.
13. A. Urakawa and A. Baiker, *Top. Catal.*, 2009, **52**, 1312-1322.
14. A. de Juan and R. Tauler, *Crit. Rev. Anal. Chem.*, 2006, **36**, 163-176.
15. A. Voronov, A. Urakawa, W. van Beek, N. E. Tsakoumis, H. Emerich and M. Rønning, *Anal. Chim. Acta*, 2014, **840**, 20-27.
16. W. H. Cassinelli, L. Martins, A. R. Passos, S. H. Pulcinelli, C. V. Santilli, A. Rochet and V. Briois, *Catal. Today*, 2014, **229**, 114-122.
17. A. Bansode, B. Tidona, P. R. von Rohr and A. Urakawa, *Catal. Sci. Technol.*, 2013, **3**, 767-778.
18. C. S. Chen, W. H. Cheng and S. S. Lin, *Appl. Catal. A - Gen.*, 2003, **238**, 55-67.
19. C. S. Chen, W. H. Cheng and S. S. Lin, *Catal. Lett.*, 2000, **68**, 45-48.
20. A. Urakawa, N. Maeda and A. Baiker, *Angew. Chem. Int. Ed.*, 2008, **47**, 9256-9259.
21. P. M. Abdala, H. Mauroy and W. van Beek, *J. Appl. Cryst.*, 2014, **47**, 449-457.
22. J. Jaumot, A. de Juan and R. Tauler, *Chemom. Intell. Lab. Syst.*, 2015, **140**, 1-12.